

# Emissions, Stability, and Flame Structure of KAUST Double Swirl Burner (KDSB) Fired With Ammonia/Methane Blends

Ayman M. Elbaz\*, Zubayr O. Hassan, Alfaisal M. Albalawi, William L. Roberts

Clean Combustion Research Center, Physical Sciences and Engineering Division, King Abdullah University of Science and Technology (KAUST), Thuwal 23955-6900, Saudi Arabia

\* [ayman.elhagrasy@kaust.edu.sa](mailto:ayman.elhagrasy@kaust.edu.sa)

## Abstract

The low reactivity and higher NO<sub>x</sub> emissions of ammonia compared to hydrocarbons limit its practical application. Therefore its implementation in the combustion and power generation systems needs a different combustor geometry, via developing new combustors or adapting the existing ones. This work studies the flame stability, NO emissions, and flame appearance of NH<sub>3</sub>/CH<sub>4</sub>/air-premixed flames fired in a combustor comprising a double swirl burner, KAUST double swirl burner (KDSB). In this configuration, a lean premixed CH<sub>4</sub>/air mixture with a mixture equivalence ratio,  $\Phi_{out}$ , was fed the outer swirl, while a mixture of NH<sub>3</sub>/CH<sub>4</sub>/air mixture was supplied to the inner swirl. The ammonia mole fraction in the inner stream,  $x_{NH_3}$ , varied from 0 (neat CH<sub>4</sub>) to 1 (neat NH<sub>3</sub>) over far rich to far lean inner stream equivalence ratio,  $\Phi_{in}$ . Under a fixed inner stream Reynolds number,  $Re_{in}$ , three outer stream Reynolds numbers were investigated,  $Re_{out}$ = 4350, 5250, and 6000. The flame stability diagram was mapped in terms of  $\Phi_{in}$  versus  $x_{NH_3}$  for  $Re_{out}$  and  $\Phi_{out}$  of 0.5, 0.6, and 0.7. The stability map shows two regions of flame instability, the flashback region, and the blowout region. Increasing  $x_{NH_3}$  modifies the flame stability by increasing the blowout limit and narrowing the flashback region. The flashback region shows less sensitivity to  $\Phi_{out}$  and  $Re_{out}$ . However, the blowout limit decreases with increasing  $\Phi_{out}$  and  $Re_{out}$ , indicating an improvement in the flame stability. Low NO emissions were achieved in this burner at  $x_{NH_3}$ =1 by either enriching or leaning  $\Phi_{in}$ . Moreover, increasing  $\Phi_{out}$  leads to a reduction in NO emissions over a wide range of  $\Phi_{in}$ , and that is by pushing the overall mixture equivalence ratio towards a stoichiometric mixture. In addition, decreasing  $Re_{out}$  shows a significant reduction of NO emissions for the lean  $\Phi_{in}$ . Increasing either  $\Phi_{in}$  or  $x_{NH_3}$  increases the flame size, which indicates the requirements for a longer residence combustion time and large combustors.

## 1. Introduction

As a fueling vector, ammonia is gaining more interest for future power generation, transportation, and heating systems. Compared to typical hydrocarbons, ammonia's low reactivity characteristics and higher NO<sub>x</sub> emissions limit its practical implementation. However, the current need for decarbonization of the energy sector puts ammonia as an energy vector and carrier at the far front, making overcoming the challenges of ammonia utilization necessary [1]. Recent experimental studies have shown that introducing swirling flow enables stable combustion of premixed or non-premixed NH<sub>3</sub> /air flames [1, 2, 3]. In NH<sub>3</sub> single-stage combustion, a specific rich mixture equivalence ratio,  $\Phi$ , led to minimum NO and NH<sub>3</sub> emissions, and was found to be 1.1 both experimentally [4] and 1.2 numerically [5]. Implementing a staged combustion concept to abate NO emissions in ammonia applications seems to have limitations in mitigating NO<sub>x</sub> emissions. This is because even if very low NO is produced in the primary rich zone, the partial oxidation of NH<sub>3</sub> and the high OH concentration in the second zone promote various NO oxidation pathways [6]. Thus, an optimization process is essential in selecting the best equivalence ratio of the primary rich stage and the global equivalence ratio, which depends on the amount of air injected in the second lean stage.

Ammonia has a lower heating value (316.84 kJ/mole) than hydrocarbon fuels, such as CH<sub>4</sub> (802.3 kJ/mole) [3]. This requires large combustors and higher volumetric flow rates of pure NH<sub>3</sub> than those used in CH<sub>4</sub> /air facilities [6]. The flame speed and ignition delay time of NH<sub>3</sub> can be enhanced by blending it with a more reactive fuel [1]; this strategy can be employed to improve the applicability of NH<sub>3</sub> in practical devices. Thus, blending NH<sub>3</sub> with CH<sub>4</sub> may be a suitable way to address the challenges associated with ammonia's relatively poor reactivity while still partially reducing CO<sub>2</sub> emissions. Various studies have considered NH<sub>3</sub>/CH<sub>4</sub> blends [7, 8]; however, NO<sub>x</sub> mitigation remains the main challenge while burning ammonia, both neat and as a blend. To decarbonize the power generation and some aspects of the transportation sectors, there is interest in gradually replacing hydrocarbon fuels with NH<sub>3</sub>. In this context, our work investigates the stability, NO emissions, and flame characteristics of a novel double-swirl burner fired with ammonia/methane.

## 2. Experimental setup and tested conditions

Fig. 1 shows a 3-D isometric view, and a schematic of the newly designed KAUST Double Swirl Burner (KDSB) used in this study. Details about the burner can be found in our previous work [9]; only a brief description is provided here. The KDSB comprises two coaxial swirling streams concentric with a central bluff body. The swirl motion is generated in the inner and outer streams via individual axial swirl generators with a blade angle of 45°, see Fig. 1 for the swirlers dimensions. The inner and outer swirlers provide different swirl numbers,  $S_g$ , of 0.72 and 0.84, respectively. A combustor of a square cross-section confines the flame, where, combustor walls are equipped with rectangular quartz windows to facilitate optical access to the flame. The combustor ends with a converging flange to a circular exhaust tube, where the exhaust gaseous concentrations were sampled from location "P". The gas sample passed through a water separator and then connected to a Testo 350 Flue Gas Analyzer with the ability to measure O<sub>2</sub>, CO<sub>2</sub>, CO, NO, and unburned hydrocarbons with a 1 ppm accuracy.

A CH<sub>4</sub>/air premixed mixture was supplied to the outer swirl, whereas various NH<sub>3</sub>/CH<sub>4</sub>/air mixtures were used for the inner swirl. The mole fraction of the NH<sub>3</sub> in the inner stream,  $x_{\text{NH}_3}$ , was defined as  $x_{\text{NH}_3} = V_{\text{NH}_3}/(V_{\text{NH}_3} + V_{\text{CH}_4})$ , where  $V_{\text{NH}_3}$  and  $V_{\text{CH}_4}$  are the volume flow rates of NH<sub>3</sub> and CH<sub>4</sub> in the inner stream, respectively. The flow rates of NH<sub>3</sub> (purity > 99.98%), CH<sub>4</sub> (purity > 99.99), and air were controlled using Brooks MFCs (SLA5800) with an uncertainty of < 1%. The inner mixtures' Reynolds number was kept constant at  $Re_{\text{in}}$  of 4250, while the corresponding Reynolds number of the outer stream ( $Re_{\text{out}}$ ) was changed to 4350, 5250, and 6000, based on their corresponding tube flow conditions and hydraulic diameters (see the dimensions in Fig. 1). Designing a stable, low NO combustor for NH<sub>3</sub>/CH<sub>4</sub>/air co-firing is essential. Thus, first, flame stability diagrams were measured under various outer stream equivalence ratios,  $\Phi_{\text{out}}$ , and various  $x_{\text{NH}_3}$  of the inner mixture. Then NO emissions over a wide range of inner stream equivalence ratios,  $\Phi_{\text{in}}$ , and  $x_{\text{NH}_3}$  were measured for given values of  $\Phi_{\text{out}}$ . Direct flame images were taken for certain flame conditions using a Nikon D700 DSLR camera fitted with a UV lens and a shutter speed of 1/s, f/8, and ISO = 500.

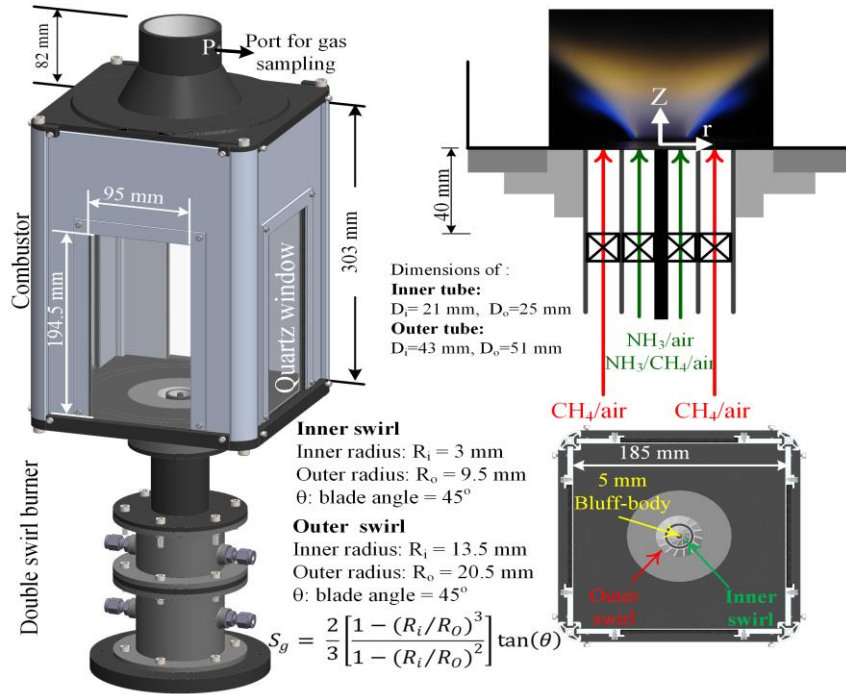


**Fig. 1.** KAUST Double Swirl Burner, KDSB

### 3. Results and discussion

#### 3.1 Stability mapping

The  $x_{\text{NH}_3}$  in the inner stream varied from 0 (pure methane) to 1 (pure ammonia) to establish the flame stability map. For a given  $x_{\text{NH}_3}$  and  $\Phi_{\text{out}}$ ,  $\Phi_{\text{in}}$  of the inner mixture was increased or decreased until either flashback or extinction of the flame were detected. Flashback was detected when the flame stabilized upstream of the bluff-body tip. The extinction region defined the minimum  $\Phi_{\text{in}}$ ,

i.e., the blowout limit to stabilize the flame. The flame stability diagrams in terms of  $\Phi_{in}$  versus  $x_{NH_3}$  at  $\Phi_{out} = 0.5, 0.6,$  and  $0.7$  for  $Re_{out} = 6000$  and  $5250$  are shown in Fig. 2a and Fig. 2b, respectively. As shown, the flame stability map is bounded by flashback and blowout regions. The flashback region (red-shaded zone) has two limits, i.e., upper and lower flashback limits, which show a broad region for pure  $CH_4$ . For a given  $Re_{out}$ , these two limits were insensitive to  $\Phi_{out}$ , thus the reported boundaries are the mean flashback boundaries for  $\Phi_{out} = 0.5, 0.6,$  and  $0.7$ . As shown the flashback region narrows with increasing  $x_{NH_3}$  and merges into a single point at  $\approx x_{NH_3}=0.4$ , where there is no flashback beyond  $x_{NH_3}=0.4$ , due to the low reactivity of  $NH_3$ . For a given  $\Phi_{out}$ ,  $\Phi_{in}$  at the blowout limit slightly increases at low  $x_{NH_3}$ , but rapidly increases at high  $x_{NH_3}$ , as seen in  $\Phi_{in}$  for  $x_{NH_3} > 0.3$  at  $\Phi_{out} = 0.6$  and  $Re_{out} = 6000$ , Fig. 2a. This is consistent with the decrease in lean flammability limits with increasing  $x_{NH_3}$ . Increasing  $NH_3\%$  in  $NH_3/CH_4$  /air flames depletes the  $O/OH$  radical pool by promoting the chain-terminating reactions by  $NH_3$  chemistry, which slows down the overall reaction and slows down the flame speed. This is consistent with the decrease in lean flammability limits with increasing  $x_{NH_3}$ . This modifies the stability diagram by increasing the lean blowout equivalence ratios and narrows the flashback region with increasing  $x_{NH_3}$ . In addition, for a given  $x_{NH_3}$  increasing  $\Phi_{out}$  enhances the flame stabilization by decreasing  $\Phi_{in}$  at the blowout limits. This behavior suggests the back support of the outer stream to the lean blowout limit. Note that no lean blowout limit was recorded at  $\Phi_{out} = 0.7$ . In addition, the higher  $\Phi_{out}$  extends the values of  $NH_3\%$  in the inner stream for a stable flame. As shown in Figs. 2a-2b, that the boundaries of the flashback region do not show significant sensitivity to  $Re_{out}$ . However, the blowout limits (as shown in Fig. 2c) show a significant reduction in  $\Phi_{in}$  with the decrease in  $Re_{out}$  from  $5250$  to  $4350$ , but a slight decrease at the decrease of  $Re_{out}$  from  $6000$  to  $5250$ .

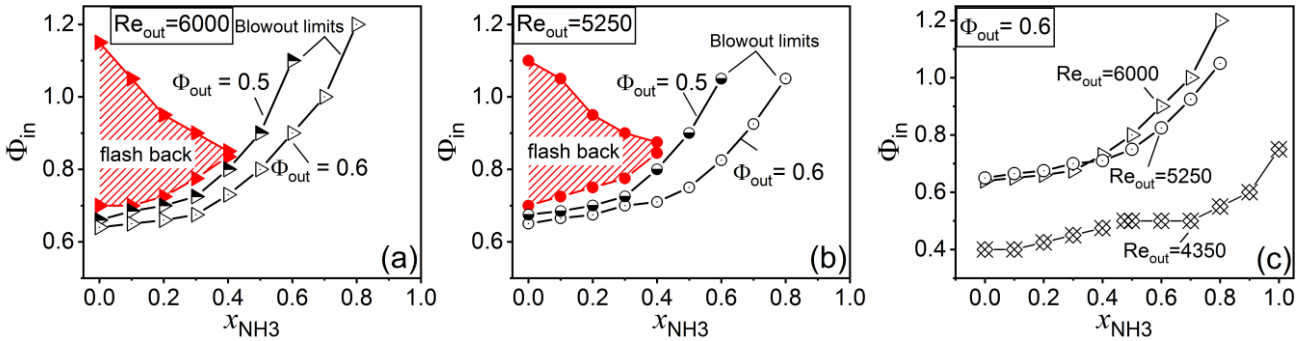


**Fig. 2.** Flame stability diagram: (a)  $\Phi_{in}$  versus  $x_{NH_3}$  at  $Re_{out}=6000$  at  $\Phi_{out}= 0.5$  and  $0.6$ , (b)  $\Phi_{in}$  versus  $x_{NH_3}$  at  $Re_{out}=5250$  at  $\Phi_{out}= 0.5$  and  $0.6$ , and (c)  $\Phi_{in}$  versus  $x_{NH_3}$   $\Phi_{out}= 0.6$  for various  $Re_{out} =4350, 5250$  and  $6000$ .

### 3.2 Exhaust NO Emissions

The impact of the inner stream blending ratio,  $x_{NH_3}$  (varies from 0 to 1) on the exhaust NO concentration at  $Re_{out} = 6000$ , and  $\Phi_{out} = 0.7$ , was investigated, where Fig. 3 shows the NO concentrations versus  $\Phi_{in}$  and the overall mixture equivalence ratio,  $\Phi_{ov}$ , ( $\Phi_{ov}$  is calculated based on the total mass flow rates of the air and fuel supplied to the burner) at different  $x_{NH_3}$ . Different trends of NO emissions were noticed with the variation of  $\Phi_{in}$  and  $x_{NH_3}$ . At  $x_{NH_3} = 0$  (shown in Fig. 3a), very low NO emissions were measured over a wide range of  $\Phi_{in}$ , in this case, the thermal/prompt NO dominates the NO formation mechanisms. Relative to pure methane flames

(i.e.,  $x_{\text{NH}_3} = 0$ ), a further increase in  $x_{\text{NH}_3}$  leads to a significant increase in the NO emissions, indicating that the fuel-NO chemistry dominates the NO formation pathway. For the mixtures with  $0 < x_{\text{NH}_3} \leq 0.75$ , the NO profiles show a peak concentration at  $\Phi_{\text{in}} = 0.8$  or  $\Phi_{\text{ov}} \approx 0.65$ , (note that at  $x_{\text{NH}_3} = 0$  or  $0.25$ , the range of investigated  $\Phi_{\text{in}}$  was limited by the flashback occurs in the inner swirl). However, for pure  $\text{NH}_3$  (i.e. at  $x_{\text{NH}_3}=1$ ), the NO profile shows low NO concentrations for the rich  $\Phi_{\text{in}}$  and gradually increase while  $\Phi_{\text{in}}$  moves towards the lean mixture.

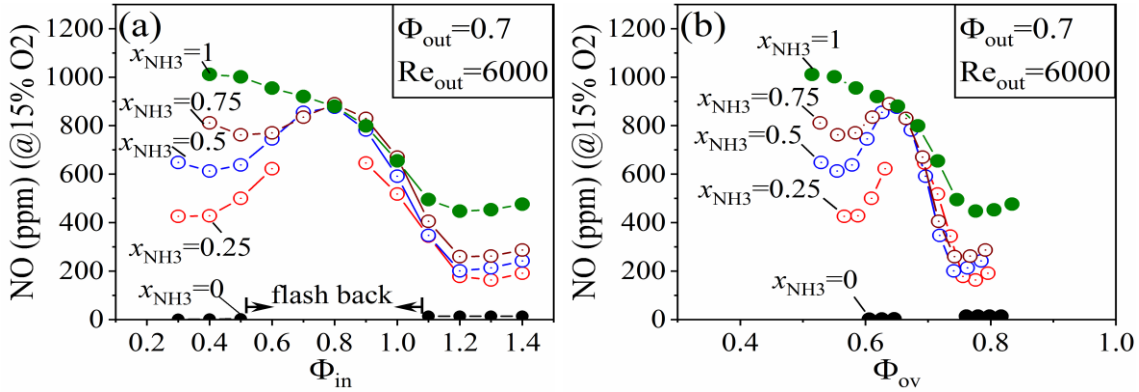


**Fig. 3.** NO emissions at  $\Phi_{\text{out}} = 0.7$  and  $\text{Re}_{\text{out}}=6000$  at various  $x_{\text{NH}_3}$ : (a) NO versus  $\Phi_{\text{in}}$ , and (b) NO versus  $\Phi_{\text{ov}}$ .

As shown for all the blends, the reduction in NO was steep increasing  $\Phi_{\text{in}}$  from 0.8 to 1.2 (see Fig. 3a), and appears more steep versus  $\Phi_{\text{ov}}$  (see Fig. 3b), indicating the high sensitivity of NO emissions to  $\Phi_{\text{ov}}$  with enriching  $\Phi_{\text{in}}$ . Also in this region, the NO was not seen to be sensitive to  $x_{\text{NH}_3}$ . However, at the substantially rich central mixture ( $\Phi_{\text{in}} > 1.2$ ), the NO concentration became less sensitive to  $\Phi_{\text{in}}$ . In addition, in this region, NO increases a little with increasing  $x_{\text{NH}_3}$  from 0.25 to 0.75 but shows an obvious increase when moving to pure  $\text{NH}_3$  at the central mixture, i.e.,  $x_{\text{NH}_3}=1$ , see Fig. 3. For  $\Phi_{\text{in}} < 0.8$ , (or  $\Phi_{\text{ov}} < 0.65$ ), and for the  $x_{\text{NH}_3} < 1$ , the decrease in  $\Phi_{\text{in}}$  and hence  $\Phi_{\text{ov}}$  leads first to a decrease in NO before it turns into a slight increase at the far lean  $\Phi_{\text{in}}$  (which is more obvious at  $x_{\text{NH}_3} = 0.75$  and  $0.5$ , Fig. 3b).

Moreover, to understand the impact of  $\Phi_{\text{out}}$  on the NO concentration, as shown in Fig. 4, for  $x_{\text{NH}_3} = 1$ , and  $\text{Re}_{\text{out}} = 6000$ ,  $\Phi_{\text{out}}$  is increased to 0.75 and 0.8. As shown as  $\Phi_{\text{out}}$  increases to 0.75 and 0.8 there is a drop in the NO concentration (at  $\Phi_{\text{in}} = 0.8$ , NO drops from 880 to 620 ppm with increasing  $\Phi_{\text{out}}$  from 0.7 to 0.8). In addition for the far lean  $\Phi_{\text{in}}$ , the NO concentration shows a decreased trend with  $\Phi_{\text{in}}$  at  $\Phi_{\text{out}} = 0.7$  and 0.8. The same observations were recorded at  $\text{Re}_{\text{out}} = 5250$  (as shown in Fig. 5), where leaning out  $\Phi_{\text{out}}$  to 0.65 leads to an increase in NO emissions. It should be noted that leaning  $\Phi_{\text{out}}$  overcomes the enriching influence of  $\Phi_{\text{in}}$ , resulting in higher NO emissions while shifting the NO peak towards leaner  $\Phi_{\text{ov}}$ , see Fig. 4b and Fig. 5b. In Fig. 5b, it can be seen the increased sensitivity of NO emissions to  $\Phi_{\text{in}}$  with the higher leaning out  $\Phi_{\text{out}}$ .

To further investigate the effects of  $\text{Re}_{\text{out}}$ , we extended our NO measurements to the flames with  $x_{\text{NH}_3}=1$  and  $\Phi_{\text{out}} = 0.7$  at  $\text{Re}_{\text{out}} = 4250$ . Figure 6 shows the NO profiles versus  $\Phi_{\text{in}}$  and  $\Phi_{\text{ov}}$  at  $\text{Re}_{\text{out}}$

= 4250, 5250, and 6000. As shown at  $\Phi_{in} = 0.8$ , the three  $Re_{out}$  cases reported nearly the same NO concentrations. However to the left of  $\Phi_{in} = 0.8$  ( $\Phi_{in} < 0.8$ ), increasing  $Re_{out}$  leads to a significant increase in NO concentration at the same  $\Phi_{in}$ . It should be noted that increasing  $Re_{out}$  for the same  $\Phi_{out}$  shifts  $\Phi_{ov}$  towards the leaner overall mixture as shown in Fig. 6b. The impact of  $Re_{out}$  shows the opposite trends for the far rich mixture,  $\Phi_{in}$  ( $\Phi_{in} > 1.2$ ), where increasing  $Re_{out}$  reduces the NO concentration, see Fig. 6a.

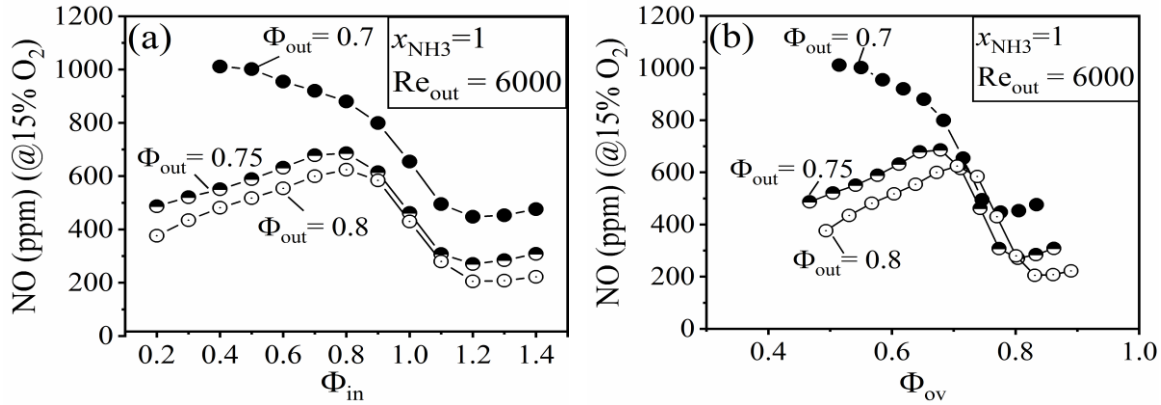


**Fig. 4.** NO emissions for  $x_{NH_3}=1$  at various  $\Phi_{out}$ : (a) NO versus  $\Phi_{in}$ , and (b) NO versus  $\Phi_{ov}$ .

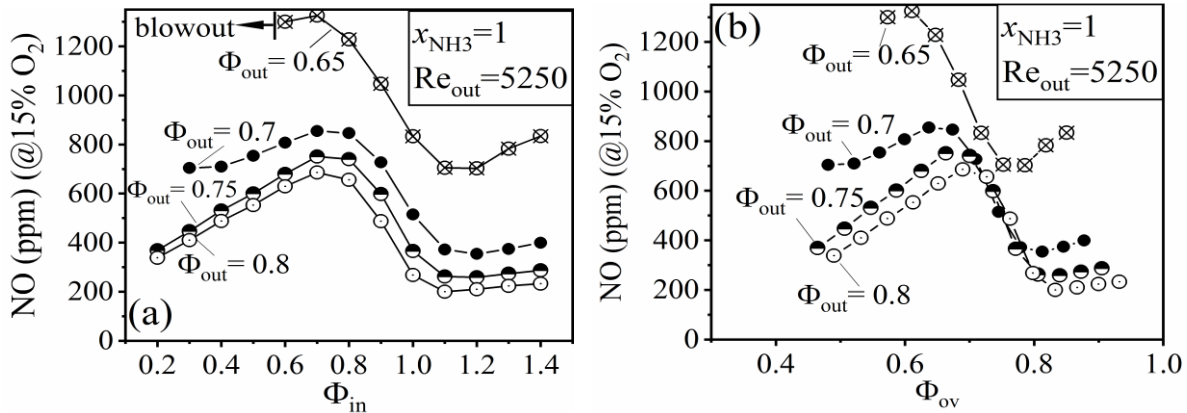


**Fig. 5.** NO emissions for  $x_{NH_3}=1$  and  $Re_{out}=5250$  at various  $\Phi_{out}$ : (a) NO versus  $\Phi_{in}$ , and (b) NO versus  $\Phi_{ov}$ .

Fuel NO formation/reduction depends on the radical pools of O/H. The preference of  $NH_3$  oxidation to form NO or  $N_2$  is determined by the competition between the reaction of amine radicals ( $NH_i$ ,  $i = 1, 2$ ) with O/OH or NO [17]. The oxidation of  $NH_i$  by the O/H radicals results in NO production predominantly via the HNO intermediate. The abundance of O and OH radicals promotes the conversion of  $NH_2$  and NH to HNO via  $NH_2 + O = HNO + H$  and  $NH + OH = HNO + H$ , which are the predominant HNO formation steps. HNO is then solely converted to NO through reactions with the O/H radicals and a dissociation reaction. Since HNO contributes to about 70% of NO production from ammonia oxidation [11], the concentration of NO in ammonia-

containing flames strongly correlates to the O and OH radical concentrations which are critical to HNO production

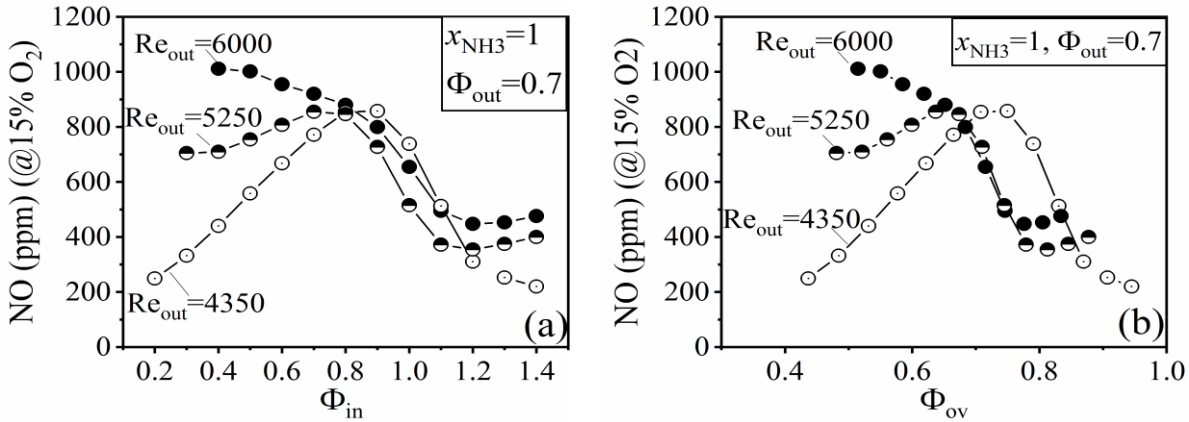


**Fig. 6.** NO emissions for  $x_{NH_3}=1$ , and  $\Phi_{out} = 0.7$  at various  $Re_{out}$ : (a) NO versus  $\Phi_{in}$ , and (b) NO versus  $\Phi_{ov}$ .

Figure 7 plots the maximum concentration of NO versus the OH, O, and H mole fractions in NH<sub>3</sub>/CH<sub>4</sub>/air flames calculated using the CEU-NH<sub>3</sub> mechanism [12] and the PREMIX module of CHEMKIN 2019 [13]. The data points in these plots were calculated for mixture equivalence ratios ranging from 0.7 to 1.4 over  $x_{NH_3}$  varying from 0 to 1 and atmospheric pressure. For the CH<sub>4</sub>-air flame ( $x_{NH_3}=0$ ) in which thermal and prompt NO formation routes are dominant, NO concentration does not correlate with the O/H radical concentration as shown in Fig. 7. However, with the addition of ammonia to methane, the fuel NO<sub>x</sub> chemistry becomes the dominant path for NO formation and hence the concentration of NO correlates with those of O and OH. On the other hand, the correlation of NO with H is dependent on the equivalence ratio, hence the plots in Fig. 7(c) do not collapse. Depending on the equivalence ratio, the contribution of H radicals to NO formation/reduction varies. The oxidation of NH<sub>2</sub> and NH by H radicals is promoted as the flame gets richer, leading to the production of N atoms which enhance NO reduction through  $N + NO = N_2 + O$  [14].

This is consistent with the results presented in Fig. 3b. To the right of the NO peak, as NH<sub>3</sub> increases, NO increases. Where the enrichment of the inner stream causes an increase in NH<sub>i</sub> radicals concentration, however, the whole mixture is in the lean composition (note that the stoichiometric A/F ratio of NH<sub>3</sub> is very low relative to CH<sub>4</sub>). However, to the left of the NO peak, the limited NH<sub>i</sub> concentration constrains the NO formation and leads to a decrease in NO concentration especially for low  $Re_{out}$  of 5250 and 4350. This is not the case with  $Re_{out} = 6000$ , where increasing  $Re_{out}$  while containing a lean mixture pushes the whole mixture away from the far lean mixture combustion, which would provide higher O/OH radicals. However, the slight increase in NO with  $x_{NH_3}$  for the far-rich central stream ( $\Phi_{in} > 1.2$ ) needs further exploration. Moreover, As  $\Phi_{out}$  decreases in the flames with  $Re_{out} = 5250$  and  $6000$  (Figs.4-5), as the peak NO concentration gradually occurs at leaner  $\Phi_{ov}$ . The impact of learning  $\Phi_{out}$  overcomes the enriching influence of  $\Phi_{in}$ , resulting in higher NO profiles and shifting the NO peak towards leaner  $\Phi_{ov}$ .

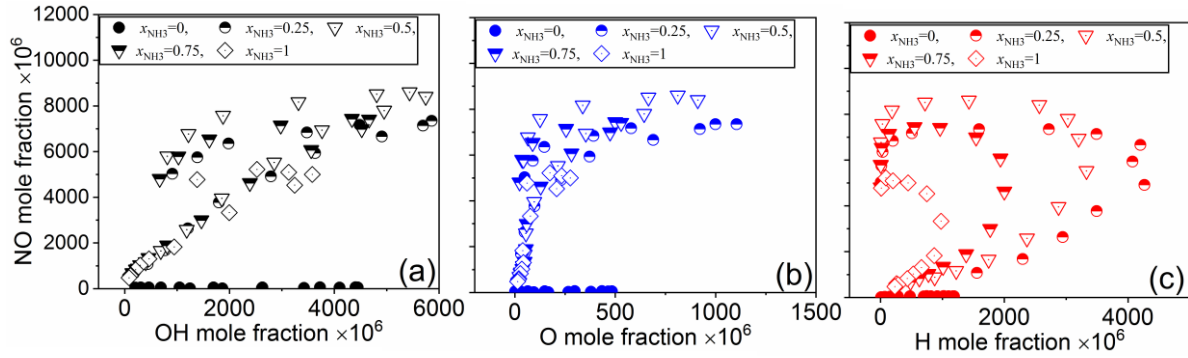


**Fig. 7.** Plots of the maximum NO concentration against the maximum concentrations of (a) OH, (b) O, and (c) H in  $\text{CH}_4$ – $\text{NH}_3$ -air flames calculated using the CEU mechanism.

### 3.2 Flame appearances

Fig. 8 shows direct images of flames at various flame conditions, where the first row (Fig. 8a-8c) shows the variation of the flame appearance with increasing  $x_{\text{NH}_3}$  from 0.2 to 1, 0.5, and 1 at  $\text{Re}_{\text{out}} = 4350$ ,  $\Phi_{\text{out}} = 0.7$ , and  $\Phi_{\text{in}} = 1.4$ . The central flame region shows orange-yellow chemiluminescence and is surrounded by an outer blue ring due to the  $\text{CH}_4$  /air outer flame. The orange-yellow color in ammonia flames is due to the  $\text{NH}_2\alpha$  and  $\text{H}_2\text{O}$  vapor bands [15]. An increase in  $x_{\text{NH}_3}$  increases the flame size, indicating the need for a longer residence time for ammonia combustors. The same observation is noted with increasing  $\Phi_{\text{in}}$ , at the same  $x_{\text{NH}_3}$  and  $\text{Re}_{\text{out}}$ , (see the second row of Fig. 8, for the flames at  $\text{Re}_{\text{out}} = 5250$ ). The impact of  $\text{Re}_{\text{out}}$  on the flames could be understood from the close inspection of the third column of Fig. 8 (Fig. 8c, 8f, 8i). As shown increasing  $\text{Re}_{\text{out}}$  from 4350 to 5250 leads to an obvious decrease in the flame length, but a slight decrease with increasing  $\text{Re}_{\text{out}}$  from 5250 to 6000. Moreover, decreasing the outer stream equivalence ratio,  $\Phi_{\text{out}}$ , from 0.7 (Fig. 8b) to 0.6 (Fig. 8h) changes the central region of the flame from yellow to orange, this may be due to the leaning out of the flame and hence higher concentration of  $\text{H}_2\text{O}$ .

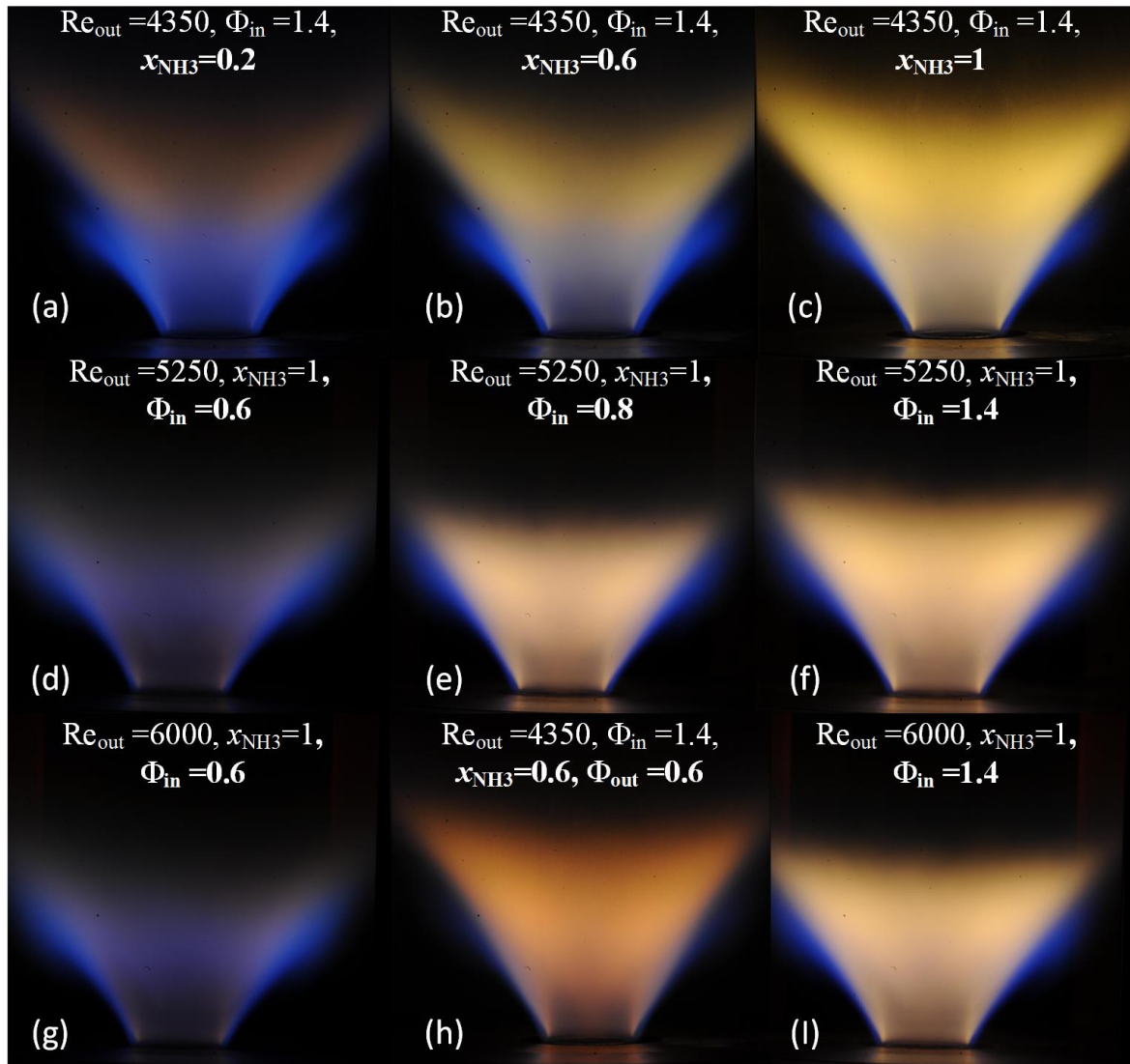


**Fig. 8.** Flame appearances at different flame conditions, all the presented cases at  $\Phi_{out} = 0.7$ , except the flame presented in Fig.8h is at  $\Phi_{out} = 0.6$ .

## Conclusions

In this work, we investigated the flame stability, NO emissions, and flame appearances of NH<sub>3</sub>/CH<sub>4</sub>-air flames fired in a double-swirl combustor. The inner swirl was supplied with NH<sub>3</sub>/CH<sub>4</sub>-air mixture, where the mole fraction of NH<sub>3</sub> in the inner fuel blend,  $x_{\text{NH}_3}$ , was varied from 0 to 1, over very lean to very rich inner stream mixture equivalence ratio ( $\Phi_{\text{in}}$  from 0.4 to 1.4). A mixture of CH<sub>4</sub>/Air was used in the outer swirl with various equivalence ratios, ( $\Phi_{\text{out}} = 0.65$  to 0.8). Cofiring NH<sub>3</sub>/CH<sub>4</sub> in the current double con- centric swirl combustor achieves a well-stable flame diagram with the ability to control NO emissions for a wide range of overall mixture equivalence ratios, ( $\Phi_{\text{ov}}$ ). The main conclusions are as follows:

1. The stability map, in terms of  $\Phi_{\text{in}}$  versus  $x_{\text{NH}_3}$ , shows that the stable flame region is bounded by a flashback and lean blowout regions. Increasing  $x_{\text{NH}_3}$  of the central stream narrows the flashback region and slightly retards the lean blowout limits. Increasing  $\Phi_{\text{out}}$  or decreasing the outer stream Reynolds number,  $Re_{\text{out}}$ , improves the lean blowout limits, whereas the flashback region is insensitive to  $\Phi_{\text{out}}$ .
2. Double swirl flames with a rich NH<sub>3</sub>/air mixture in the central swirl and a lean CH<sub>4</sub>/air mixture in the outer swirl can result in stable, low NO emission and high combustion efficiency flames, through the precise control of  $Re_{\text{out}}$ ,  $\Phi_{\text{in}}$ ,  $\Phi_{\text{out}}$ ,  $x_{\text{NH}_3}$  and hence  $\Phi_{\text{ov}}$ .
3. Low NO emissions were achieved in this burner at  $x_{\text{NH}_3}=1$  by either enriching or leaning  $\Phi_{\text{in}}$ . Moreover, increasing  $\Phi_{\text{out}}$  leads to a reduction in NO emissions over a wide range of  $\Phi_{\text{in}}$ , and that is by pushing the overall mixture equivalence ratio towards a stoichiometric mixture.
4. Decreasing the outer stream Reynolds number,  $Re_{\text{out}}$ , leads to a significant reduction of NO emissions, and that is specifically for the lean mixture inner stream mixture.
5. Increasing either  $\Phi_{\text{in}}$  or  $x_{\text{NH}_3}$  increases the flame size, which indicates the requirements for a longer residence combustion time and large combustors.

## References

1. Elbaz, A.M., Wang, S., Guiberti, T.F. and Roberts, W.L., 2022. Review on the recent advances on ammonia combustion from the fundamentals to the applications. *Fuel Communications*, 10, p.100053.
2. Franco, M.C., Rocha, R.C., Costa, M. and Yehia, M., 2021. Characteristics of NH<sub>3</sub>/H<sub>2</sub>/air flames in a combustor fired by a swirl and bluff-body stabilized burner. *Proceedings of the Combustion Institute*, 38(4), pp.5129-5138.
3. Okafor, E.C., Somarathne, K.K.A., Hayakawa, A., Kudo, T., Kurata, O., Iki, N. and Kobayashi, H., 2019. Towards the development of an efficient low-NO<sub>x</sub> ammonia combustor for a micro gas turbine. *Proceedings of the combustion institute*, 37(4), pp.4597-4606.
4. Ichikawa, A., Naito, Y., Hayakawa, A., Kudo, T. and Kobayashi, H., 2019. Burning velocity and flame structure of CH<sub>4</sub>/NH<sub>3</sub>/air turbulent premixed flames at high pressure. *International Journal of Hydrogen Energy*, 44(13), pp.6991-6999.
5. Somarathne, K.D.K.A., Hatakeyama, S., Hayakawa, A. and Kobayashi, H., 2017. Numerical study of a low emission gas turbine like combustor for turbulent ammonia/air premixed swirl flames with a secondary air injection at high pressure. *International Journal of Hydrogen Energy*, 42(44), pp.27388-27399.
6. Somarathne, K.D.K.A., Okafor, E.C., Hayakawa, A., Kudo, T., Kurata, O., Iki, N. and Kobayashi, H., 2019. Emission characteristics of turbulent non-premixed ammonia/air and methane/air swirl flames

through a rich-lean combustor under various wall thermal boundary conditions at high pressure. *Combustion and flame*, 210, pp.247-261.

7. Zhang, M., An, Z., Wei, X., Wang, J., Huang, Z. and Tan, H., 2021. Emission analysis of the CH<sub>4</sub>/NH<sub>3</sub>/air co-firing fuels in a model combustor. *Fuel*, 291, p.120135.
8. Okafor, E.C., Somarathne, K.K.A., Ratthan, R., Hayakawa, A., Kudo, T., Kurata, O., Iki, N., Tsujimura, T., Furutani, H. and Kobayashi, H., 2020. Control of NO<sub>x</sub> and other emissions in micro gas turbine combustors fuelled with mixtures of methane and ammonia. *Combustion and flame*, 211, pp.406-416.
9. Elbaz, A.M., Albalawi, A.M., Wang, S. and Roberts, W.L., 2023. Stability and characteristics of NH<sub>3</sub>/CH<sub>4</sub>/air flames in a combustor fired by a double swirl stabilized burner. *Proceedings of the Combustion Institute*, 39(4), pp.4205-4213.
10. Glarborg, P., Miller, J.A., Ruscic, B. and Klippenstein, S.J., 2018. Modeling nitrogen chemistry in combustion. *Progress in energy and combustion science*, 67, pp.31-68.
11. Lindstedt, R.P., Lockwood, F.C. and Selim, M.A., 1994. Detailed kinetic modelling of chemistry and temperature effects on ammonia oxidation. *Combustion science and technology*, 99(4-6), pp.253-276.
12. Wang, S., Wang, Z., Chen, C., Elbaz, A.M., Sun, Z. and Roberts, W.L., 2022. Applying heat flux method to laminar burning velocity measurements of NH<sub>3</sub>/CH<sub>4</sub>/air at elevated pressures and kinetic modeling study. *Combustion and Flame*, 236, p.111788.
13. CHEMKIN-Pro., "R2, ANSYS", San Diego, (2019).
14. Kobayashi, H., Hayakawa, A., Somarathne, K.K.A. and Okafor, E.C., 2019. Science and technology of ammonia combustion. *Proceedings of the combustion institute*, 37(1), pp.109-133.
15. Hayakawa, A., Goto, T., Mimoto, R., Arakawa, Y., Kudo, T. and Kobayashi, H., 2015. Laminar burning velocity and Markstein length of ammonia/air premixed flames at various pressures. *Fuel*, 159, pp.98-106.